Sensors and Materials, Vol. 34, No. 9 (2022) 3607–3621
MYU Tokyo

S & M 3064

Synchronizations of Nerve-cell Systems via Adaptive Integral-type Quick-time Stabilized Sliding Mode Control Approach

Deqian Zhang, Chi-Hsin Yang,* Ruiwei Li, Pu Li, and Kun-Chieh Wang

School of Intelligent Engineering, Shaoguan University, Shaoguan City, Guangdong Province 512005, China

(Received July 4, 2022; accepted September 15, 2022)

Keywords: synchronization, integral-type quick-time stabilized sliding mode, adaptive control, space-clamped FitzHugh–Nagumo (SFHN) neuron, voltage-sensing equipment

Adaptive sliding mode control with an online updated gain algorithm based on a newly defined integral-type quick-time stabilized sliding mode (IQSSM) is proposed for complete or anti-synchronization between two nerve-cell systems, despite the influences of system uncertainties and external disturbances. The global and quick finite-time stability for the IQSSM is proven to support the hypothesis that the overall designed closed-loop control system can achieve the control goal. Moreover, the proposed control scheme can solve two kinds of control problems for synchronization simply by suitably tuning the design parameters. The developed control schemes can be implemented by a hardware circuit with voltage-sensing equipment.

1. Introduction

Motivated by the pioneering work on synchronization between two identical chaotic systems,[1] the research on the complete and anti-synchronization of nerve-cell systems has played an important role in understanding biological systems. These types of synchronization are helpful in fully comprehending the functions of human brain information processes and artificial neural circuits. Both types of synchronization have been widely studied in the field of neuroscience.[2–14] The control technologies for solving synchronization problems include nonlinear control,[2] the robust output feedback method,[3] the linear matrix inequality (LMI)-based adaptive control method,[4] sliding mode control schemes,[5,7,8] the adaptive backstepping control scheme,[6] and time delay methods.[10,14]

To understand the dynamical behaviors of nerve-cell neurons, the Hodgkin–Huxley (HH) model[15,16] is a relatively complete model used to explain the fundamental principles of ionic mechanisms through the membrane of a neuron. However, the HH model involves four states and includes many system parameters, increasing the difficulty of its application. To simplify this analytical approach, the FitzHugh–Nagumo (FHN) neuron model[17,18] and space-clamped FitzHugh–Nagumo (SFHN) neuron model,[19] which are simplified forms derived from the HH model, are more convenient for studying the dynamics of a neuron.

*Corresponding author: e-mail: yang20227002@sgu.edu.cn
https://doi.org/10.18494/SAM4023

ISSN 0914-4935 © MYU K.K.
https://myukk.org/

The following isolated SFHN neuron system, which is subjected to an external electric stimulation (EES) and mainly follows the model introduced in Ref. 19, is expressed by the following second-order non-autonomous differential equations with respect to the dimensionless time t:[20]

$$\begin{cases} \dot{x}_1 = x_1(1-x_1)(x_1-A) - y_1 + K_1\cos(\omega_1 t) + I_1, \\ \dot{y}_1 = B(Cx_1 - y_1), \end{cases} \tag{1}$$

where the state variable x_1 is the rescaled action potential and the state variable y_1 is the rescaled generalized recovery variable. The system parameters A, B, C are positive constants that affect the behavior of the system. $K_1\cos(\omega_1 t)$ represents the EES with amplitude K_1 and period $T_1 = 2\pi/\omega_1$. I_1 is the ionic current. An isolated SFHN neuron subjected to an EES is expected to exhibit various nonlinear behaviors. It is known that, for certain values of system parameters K_1, ω_1, and I_1, the neuron undergoes a complicated chaotic firing.[20] For the normal set of parameters of the system, $A = 0.25$, $B = 0.02$, $C = 0.25$, $K_1 = 0.055$, $\omega_1 = 0.1$, $I_1 = 0.082$, the SFHN neuron exhibits chaotic dynamics.[21]

To investigate the chaotic dynamical system of an SFHN neuron, circuit implementations are usually applied in practice. Moreover, due to its flexibility, real-time processing, and straightforward analysis, the SFHN neuron by analogy with an electrical circuit is suitable for applications. Hardware realizations by analog electronic circuits,[22,23] VLSI,[24] and a field-programmable analog array[25] have been reported. The technologies of voltage-sensing systems have been reported to enable practical uses of the SFHN neuron.[26,27] The state variables of an SFHN neuron are analogized by the corresponding voltages in the circuits and, therefore, the time responses of an electrical SFHN neuron circuit for feedback control can be sensed by applying suitable voltage-sensing equipment. Furthermore, the control schemes developed for synchronization are also applied in the hardware circuit realization using sensing equipment.[28]

In past studies of complete synchronization in biological systems such as nerve-cell neurons[2–4] and coronary artery systems,[29,30] the addressed control schemes were usually associated with the active control parts to directly cancel the nonlinear terms of the error system. Indeed, the directed cancelation involved in the designed control scheme is mainly caused by the chattering effect, and the scheme has insufficient robustness to tackle system uncertainties. To cope with the nonlinear terms when controlling synchronization, an adaptive technology was applied to obtain good performance by utilizing the fact that the phase trajectories are bounded in biological systems,[31] where self-tuning terminal sliding mode control was introduced. Motivated by previous works,[5,31] in this study, we consider the control problems of complete and anti-synchronization between two isolated SFHN neurons with different ionic currents and EESs.

The novelty, features, and main contributions of this study are listed below.

(1) In the previous work on synchronizations of SFHN neurons,[2–8] it was assumed that two nerve-cell systems have the same EES $K_1\cos(\omega_1 t)$ and ionic current I_1 in Eq. (1). In this study, the control problem of synchronizations between two chaotic SFHN neurons with two different values of EES and ionic current is discussed. This is a more practical problem but also more complicated.

(2) To solve the control problem of complete and anti-synchronization between two SFHN neurons, a novel integral-type quick-time stabilized sliding mode (IQSSM) is defined and its stability is examined. The dynamical behavior of the defined IQSSM is that on a sliding surface. One of the state variables of the error system is first stabilized within a finite time. Then, the other state variable is exponentially stabilized. A detailed proof of the stability is given.
(3) Different from in past works,[2–8] complete or anti-synchronization requires the adaption of specific and different types of control schemes to achieve the control goal. In this study, the robust adaptive IQSSM control scheme is developed. It can simultaneously solve the control problems of complete or anti-synchronization by simply suitably adjusting the design parameters involved in the control scheme.
(4) The proposed adaptive IQSSM control scheme contains three time-varying state feedback gains, which can adaptively compensate the effects of nonlinear terms in the synchronized error dynamical system. These time-varying feedback gains are updated online using established algorithms. On the basis of Lyapunov stability theory, sufficient conditions are provided to guarantee the stability of the control problems for the two types of synchronization. In addition, numerical simulations are carried out to validate the performance of the proposed control scheme.

The contents of the paper are as follows. The control problems for complete and anti-synchronization between two isolated SFHN neurons are formulated in Sect. 2. In Sect. 3, the novel IQSSM and its quick and finite-time stabilization are analyzed. In addition, the design procedures of the adaptive IQSSM control scheme for achieving complete or anti-synchronization are developed. Furthermore, the proof of stability for the closed-loop control system is also provided. Numerical simulations are carried out to demonstrate the performance of the proposed control scheme in Sect. 4. Finally, some concluding remarks are made.

2. Formulation of Control Problems for Synchronizations

We consider the formulation of control problems for complete and anti-synchronization between two isolated SFHN neurons with different EESs and ionic currents. The drive SFHN neuron is expressed in the form of Eq. (1) with a system uncertainty $D(x_1, y_1)$ and an external disturbance $E(t)$ added to the first equation of Eq. (1). The slave SFHN neuron is isolated and modeled using the same form of Eq. (1) with the designed control input $\phi(t)$ added as follows:

$$\begin{cases} \dot{x}_2 = x_2(1-x_2)(x_2-A) - y_2 + K_2\cos(\omega_2 t) + I_2 + \phi(t), \\ \dot{y}_2 = B(Cx_2 - y_2), \end{cases} \tag{2}$$

where x_2, y_2 are the state variables of the slave neuron. $K_2\cos(\omega_2 t)$ represents the EES with amplitude K_2 and period $T_2 = 2\pi/\omega_2$ and I_2 is the ionic current.

By assuming the different EESs and ionic currents for the SFHN neurons in Eqs. (1) and (2), that is, $K_2 \neq K_1$, $I_2 \neq I_1$, $\omega_2 \neq \omega_1$, the control problems for the synchronizations are formulated. Otherwise, we also assume that the drive and slave neurons in Eqs. (1) and (2) have unique solutions for any given initial conditions. They can still produce the bounded dynamical phase

trajectories in the effects of the system uncertainty $D(x_1, y_1)$, external disturbance $E(t)$, and control input $\phi(t)$.

Synchronous error states between the neurons in Eqs. (1) and (2) are defined as follows:

$$\theta_x(t) = x_2(t) - \lambda x_1(t), \quad \theta_y(t) = y_2(t) - \lambda y_1(t), \tag{3}$$

where $\lambda \in \{-1, 1\}$ is a scaling factor that defines the type of synchronization between the synchronous neurons: $\lambda = 1$ for complete synchronization and $\lambda = -1$ for anti-synchronization. The control problem considered in this paper is to propose an appropriate control scheme $\phi(t)$ that synchronizes or anti-synchronizes the states of the drive neuron in Eq. (1) and the slave neuron in Eq. (2), that is, $\lim_{t\to\infty}|\theta_x(t)| \to 0$, $\lim_{t\to\infty}|\theta_y(t)| \to 0$, for any initial conditions.

By taking the derivative of Eq. (3) with respect to the dimensionless time t, the error state equations in the synchronizations are expressed as

$$\begin{cases} \dot{\theta}_x(t) = [\Psi_1(x_1, x_2) + (A+1)\Psi_2(x_1, x_2) - A]\theta_x(t) - \theta_y(t) \\ \qquad + \lambda(\lambda+1)(1-\lambda)x_1^3 + \lambda(\lambda-1)(A+1)x_1^2 + K_2\cos(\omega_2 t) \\ \qquad - \lambda K_1\cos(\omega_1 t) + (I_2 - \lambda I_1) - \lambda(D(x_1, y_1) + E(t)) + \phi(t), \\ \dot{\theta}_y(t) = B(C\theta_x(t) - \theta_y(t)), \end{cases} \tag{4}$$

where the functions are $\Psi_1(x_1, x_2) = -(\lambda^2 x_1^2 + \lambda x_1 x_2 + x_2^2)$ and $\Psi_2(x_1, x_2) = \lambda x_1 + x_2$. Because the phase trajectories of $x_1(t)$, $x_2(t)$ for the drive and slave neurons are bounded, it is assumed that $\Psi_i(x_1, x_2), i = 1, 2$ satisfy

$$0 < |\Psi_1(x_1, x_2)| < N_1, \ 0 < |\Psi_2(x_1, x_2)| < N_2. \tag{5}$$

For the control design, $\Psi_i(x_1, x_2), i = 1, 2$ are the time-varying gains versus the dimensionless time t of the synchronous error state $\theta_x(t)$. They are handled using the adaptive method without their direct elimination in the study.

3. Adaptive Control by Novel Integral-type Quick-time Stabilized Sliding Mode

In this section, an adaptive control scheme based on a novel IQSSM for synchronization between two isolated SFHN neurons is constructed in accordance with the system in Eq. (4). Before giving the main results, the key lemma used to examine the quick finite-time stability is first introduced.

Lemma:[32] For the dynamical system of $u(t)$ satisfying

$$\dot{u}(t) = -\rho[u(t)]^{2-q/p} - \gamma[u(t)]^{q/p}, \tag{6}$$

where $\rho > 0$, $\gamma > 0$, and q, p are positive odd integers with $0 < q/p < 1$, the global and finite-time stability for a given initial condition $u(0) = u_0 \neq 0$ is guaranteed. Furthermore, for $\forall\, u_0 \neq 0$, $u(t) = 0$ is reached at time

$$T_s(u_0) = \frac{p}{(p-q)\sqrt{\rho\gamma}} \arctan\left[\sqrt{\frac{\rho}{\gamma}}(u_0)^{(p-q)/p}\right] > 0 \tag{7}$$

and remains zero for $\forall\, t \geq T_s(u_0) > 0$. Moreover, the finite time $T_s(u_0)$ has a maximum value $T_s(\infty)$ given by

$$T_s(\infty) = \lim_{u_0 \to \infty} T_s(u_0) = \frac{\pi p}{2(p-q)\sqrt{\rho\gamma}} > 0. \tag{8}$$

Remark 1.

The details of the proof are omitted here but are given in Lemma 4.1 of Ref. 32. It is obvious that the maximum value $T_s(\infty)$ is only dependent on the design parameters ρ, γ, q, p and is applied to estimate the convergence time of the controlled system.

Two steps of the designed adaptive IQSSM control are provided here. First, a novel IQSSM $s(t)$ is defined and the characteristics of stabilization are discussed. Second, an adaptive control scheme based on the IQSSM with adaption algorithms is developed such that the phase trajectory of synchronous error states can arrive at the sliding surface $s(t) = 0$ and remain there, $\dot{s}(t) = 0$, despite external disturbances and system uncertainties.

The novel IQSSM $s(t)$ is defined by

$$s(t) = [\theta_x(t)]^{m/n} + \alpha \int_{\tau=0}^{t} [\theta_x(\tau)]^{2m/n-1} d\tau + \frac{1}{\beta}\left[\theta_y(t) + B\int_{\tau=0}^{t} \theta_y(\tau) d\tau\right], \tag{9}$$

where $\alpha, \beta > 0$ and m and n are positive odd integers with $1 < m/n < 2$. The stability on the sliding surface $s(t) = 0$ is discussed in the following. Theorem 1 is provided as a criterion to guarantee the quick finite-time stability of the novel IQSSM in Eq. (9).

Theorem 1.

For the IQSSM $s(t)$ defined in Eq. (9) associated with the second equation in Eq. (4), the global and quick finite-time stability of the state $\theta_x(t)$ is guaranteed for $s(t) = 0$ and $\dot{s}(t) = 0$. First, it converges to the origin $\theta_x(t) = 0$ at the finite time given by

$$t_s = \frac{m\sqrt{\beta}}{(m-n)\sqrt{\alpha BC}} \arctan\left(\sqrt{\frac{\alpha\beta}{BC}}\left[\theta_x(t_0)\right]^{m/n-1}\right) + t_0. \tag{10}$$

It then remains on $\theta_x(t) = 0\ \forall\ t \geq t_s > 0$, where $t_0 > 0$ is the time of the phase trajectory of $\theta_x(t)$, $\theta_y(t)$ from the given initial conditions $\theta_y(0)$, $\theta_y(0)$ to the arrival at the sliding surface $s(t) = 0$. Furthermore, for the case of $\theta_x(t_0) \to \infty$, the finite time has a maximum value given by

$$t_{s\_\max} = \frac{\pi m\sqrt{\beta}}{2(m-n)\sqrt{\alpha BC}} + t_0. \tag{11}$$

Then, the state $\theta_y(t)$ is stabilized exponentially.

Proof.

For the given initial conditions $\theta_x(0)$, $\theta_y(0)$, when the sliding surface $s(t) = 0$ is reached and $\theta_x(t)$, $\theta_y(t)$ remain on it, $\dot{s}(t) = 0$ is satisfied, and the system dynamics of Eq. (9) is equivalently transformed to the following nonlinear differential equation by substituting the second equation in Eq. (4):

$$\begin{aligned} &\dot{s}(t) = \frac{m}{n}\left[\theta_x(t)\right]^{m/n-1}\dot{\theta}_x(t) + \alpha\left[\theta_x(t)\right]^{2m/n-1} + \frac{1}{\beta}\left[\dot{\theta}_y(t) + B\theta_y(t)\right] = 0 \\ &\Rightarrow \dot{\theta}_x(t) + \frac{\alpha n}{m}\left[\theta_x(t)\right]^{m/n} + \frac{BCn}{\beta m}\left[\theta_x(t)\right]^{2-m/n} = 0, \end{aligned} \tag{12}$$

where $0 < 2 - (m/n) < 1$ for $1 < m/n < 2$. The initial condition of Eq. (12) is denoted by $\theta_x(t_0) \neq 0$.

By applying the lemma and setting the corresponding parameters to $q/p = 2 - m/n$, $\rho = \alpha n/m$, $\gamma = BCn/\beta m$, it is found that the global and quick finite-time stability of $\theta_x(t)$ is obtained, and the finite time t_s required to move from $\theta_x(t_0) \neq 0$ to $\theta_x(t_s) = 0$ is evaluated using Eqs. (7) and (10). The maximum value t_{s_max} in Eq. (11) is easily derived by noting that $\lim_{\tau\to\infty} \arctan(\tau) = \pi/2$.

Furthermore, when $\theta_x(t) = 0$, $\forall\ t \geq t_s > 0$ holds, it is clear that the exponential stability of $\theta_y(t)$ with $\theta_x(t) = 0$, $\forall\ t \geq t_s > 0$ is guaranteed for the second initial condition $\theta_y(t_s) \neq 0$ because

$$\theta_y(t) + B\theta_y(t) = 0 \Rightarrow \theta_y(t) = \theta_y(t_s)\exp(-Bt),\ \ \forall t \geq t_s > 0,\ \ B > 0. \tag{13}$$

This completes the proof of **Theorem 1**.

Remark 2.

It is clear that the finite time t_s in Eq. (10) is tuned by the parameters α, $\beta > 0$. However, the value of t_s is dominated by the parameter $\alpha > 0$. The control performance depends on choosing a suitable value of $\alpha > 0$, as discussed in Sect. 4.

The adaptive IQSSM control with adaption algorithms based on the IQSSM in Eq. (9) is now proposed as Theorem 2, which provides the condition to force the phase trajectory of $\theta_x(t)$, $\theta_y(t)$ in the system given by Eq. (4) to reach the sliding surface $s(t) = 0$ and remain there in the presence of system uncertainty and an external disturbance.

Theorem 2.

For the dynamical system in Eq. (4), the adaptive IQSSM control scheme $\phi(t) = \phi_{eq}(t) + \phi_{sw}(t)$ is designed with

$$\begin{aligned} \phi_{eq}(t) &= -\frac{\alpha n}{m}\left[\theta_x(t)\right]^{m/n} - \frac{BCn}{\beta m}\left[\theta_x(t)\right]^{2-m/n}, \\ \phi_{sw}(t) &= -\left[k_1(t) + k_2(t)\left|\theta_x(t)\right| + k_3(t)\left|\theta_y(t)\right|\right] \cdot sign(s(t)), \end{aligned} \tag{14}$$

where $s(t)$ is the IQSSM in Eq. (9). The parameters are restricted for $\alpha > 0$, $\beta > 0$, m, n are positive odd integers with 1 , $m/n < 2$, and sign(•) denotes the sign function. The adaptive feedback gains $k_i(t)$, $i = 1, 2, 3$ are tuned online using the following algorithms:

$$\begin{aligned} \dot{k}_1(t) &= \mu_1 \left|s(t)\right|\left|\theta_x(t)\right|^{m/n-1}, \quad k_1(0) = 0, \quad \mu_1 > 0, \\ \dot{k}_2(t) &= \mu_2 \left|s(t)\right|\left|\theta_x(t)\right|^{m/n}, \quad k_2(0) = 0, \quad \mu_2 > 0, \\ \dot{k}_3(t) &= \mu_3 \left|s(t)\right|\left|\theta_x(t)\right|^{m/n-1}\left|\theta_y(t)\right|, \quad k_3(0) = 0, \quad \mu_3 > 0. \end{aligned} \tag{15}$$

Therefore, $\theta_x(t)$, $\theta_y(t)$ in the system in Eq. (4) reaches the sliding surface $s(t) = 0$ and remains there. This shows that the state $\theta_x(t)$ tends to zero within a finite time and the other state $\theta_y(t)$ is stabilized exponentially. This completes the synchronization between the SFHN neurons in Eqs. (1) and (2).

Proof.

The positive candidate of the Lyapunov function is defined by

$$L(t) = \frac{1}{2}s^2(t) + \sum_{i=1}^{3}\frac{m}{2n\mu_i}(k_i(t) - g_i)^2 \geq 0, \tag{16}$$

where $g_i > 0$, $i = 0, 1, 2$ are positive constants satisfying

$$\begin{aligned} &g_1 > N_3 + K_2 + \left|\lambda\right|K_1 + I_2 + \left|\lambda\right|I_1 + \left|\lambda\right|(\left|D(x_1, y_1)\right| + \left|E(t)\right|), \\ &g_2 > N_1 + (A+1)N_2 + A, \\ &g_3 > 1, \end{aligned} \tag{17}$$

with $0 \leq \left|\lambda(\lambda-1)x_1^2 + \lambda(1-\lambda)(\lambda+1)x_1^3\right| < N_3$, $\lambda \in \{-1, 1\}$. Taking the derivative of Eq. (16) with respect to the dimensionless time t associated with Eq. (4), the sliding mode defined in Eq. (9), and the adaptive IQSSM control scheme in Eqs. (14) and (15), we obtain

$$\begin{aligned}\dot{L}(t) &= s(t)\dot{s}(t) + \sum_{i=1}^{3} \frac{m}{n\mu_i}(k_i(t) - g_i)\dot{k}_i(t) \\ &= s\left[\frac{m}{n}[\theta_x]^{m/n-1}\dot{\theta}_x + \alpha[\theta_x]^{2m/n-1} + \frac{1}{\beta}\left(\dot{\theta}_y + B\theta_y\right)\right] + \frac{m}{n}\sum_{i=1}^{3}\frac{k_i(t) - g_i}{\mu_i}\dot{k}_i(t),\end{aligned}$$

$$\begin{aligned}\Rightarrow \dot{L}(t) = s\frac{m}{n}[\theta_x]^{m/n-1} \cdot \Big[&\left(\Psi_1(x_1, x_2) + (A+1)\Psi_2(x_1, x_2) - A\right)\theta_x - \theta_y \\ &+ \lambda(1-\lambda)(\lambda+1)x_1^3 + \lambda(\lambda-1)x_1^2 + K_2\cos(\omega_2 t) - \lambda K_1\cos(\omega_1 t) \\ &+ (I_2 - \lambda I_1) - \lambda(D(x_1, y_1) + E(t)) \\ &- \left(k_1(t) + k_2(t)|\theta_x| + k_2(t)|\theta_y|\right)\cdot \mathrm{sign}(s)\Big] \\ &+ \frac{m}{n}\sum_{i=1}^{3}\frac{k_i(t) - g_i}{\mu_i}\dot{k}_i(t),\end{aligned} \tag{18}$$

$$\begin{aligned}\Rightarrow \dot{L}(t) \le \frac{m}{n}|\theta_x|^{m/n-1}|s| \cdot \Big[&-\left(g_1 - N_3 - K_2 - |\lambda|K_1 - I_2 - |\lambda|I_1 - |\lambda|(|D| + |E|)\right) \\ &-\left(g_1 - N_1 - (A+1)N_2 - A\right)|\theta_x| - \left(g_2 - 1\right)|\theta_y|\Big] < 0.\end{aligned} \tag{19}$$

It is shown that $L(t)$ is a positive definite function from Eq. (16) and a decreasing function with respect to t, as can be seen from Eqs. (17) and Eq. (19). It follows that the original equilibriums ($s(t) = 0$, $k_i(t) = g_i$, $i = 0, 1, 2$) are globally asymptotically stable. It turns out that the phase trajectories of $\theta_x(t)$, $\theta_y(t)$ in system Eq. (4) asymptotically approach and remain on the sliding surface $s(t) = 0$ and that $\dot{s}(t) = 0$ from the given initial conditions $\theta_x(0)$, $\theta_y(0)$ by applying the adaptive IQSSM control scheme in Eqs. (14) and (15).

$\theta_x(t)$ is first stabilized on the sliding surface $s(t) = 0$ with $\dot{s}(t) = 0$ within a finite time t_s, which is evaluated approximately by suitably choosing α, $\beta > 0$ and positive odd m and n with $1 < m/n < 2$ in accordance with Eq. (10). Then, from Theorem 1, the exponential stabilization of $\theta_y(t)$ is guaranteed. Therefore, the synchronization between two isolated SFHN neurons in Eqs. (1) and (2) is accomplished for $\lambda \in \{-1, 1\}$, completing the proof.

Remark 3.

The synchronous error state $\theta_y(t)$ in the system in Eq. (4) is compensated adaptively without applying the equivalent control part of the proposed sliding mode control scheme. Moreover, the nonlinear functions $\Psi_i(x_1, x_2)$, $i = 1, 2$ are handled using adaptive technology.

Remark 4.

The control scheme in Eq. (14) includes discontinuous controls. To reduce the chattering phenomenon, the sign function in Eq. (14) is changed to $\tanh(\sigma/\delta)$, where δ is a sufficiently small constant. This change is applied in all the numerical experiments.

4. Numerical Simulations

The simulation code and its execution to validate the proposed adaptive IQSSM control are discussed in this section. For the calculations, the MATLAB Simulink software is used with its Runge–Kutta ode45 solver with a variable step length of integration with tolerance 10^{-8}. Two cases of numerical simulations for $\lambda \in \{-1, 1\}$ are performed, where $\lambda = 1$ for complete synchronization and $\lambda = -1$ for anti-synchronization. We also demonstrate that the two cases of synchronization problems can be solved by applying one type of adaptive control scheme by simply suitably tuning the designed parameters. The simulation parameters of the numerical simulations are listed in Table 1.

The numerical simulations are set up so that the drive and slave neurons are moving individually without control at $t = 0$. Then, the control input of the slave neuron is turned on at $t = 320$ to start the complete or anti-synchronization between the two neurons.

For the case of $\lambda = 1$ (complete synchronization) with $\alpha = 1.25$, $\mu_1 = 20$, $\mu_2 = 0.35$, $\mu_3 = 9$, the phase plane dynamics of the IQSSM $s(t)$ versus $\theta_x(t)$ and $\theta_y(t)$ is depicted in Fig. 1. It is shown

Table 1
Simulation parameters used in coding.

Name of parameter	
Initial conditions	$(x_1, y_1) = (-0.5, 0.75)$ $(x_2, y_2) = (1.0, 0.6)$
SFHN neuron parameters	$A = 0.25$, $B = 0.02$, $C = 0.25$ $K_1 = 0.055$, $\omega_1 = 0.1$, $I_1 = 0.1$ $K_2 = 0.06$, $\omega_2 = 0.15$, $I_2 = 0.082$
System uncertainty	$D(x_1, y_1) = 0.15 \cdot \sin(0.05\pi t)$
External disturbance	$E(t) = 0.15 \cdot \sin(0.05\pi t)$
Design parameters	$m = 31$, $n = 19$, $\beta = 0.005$

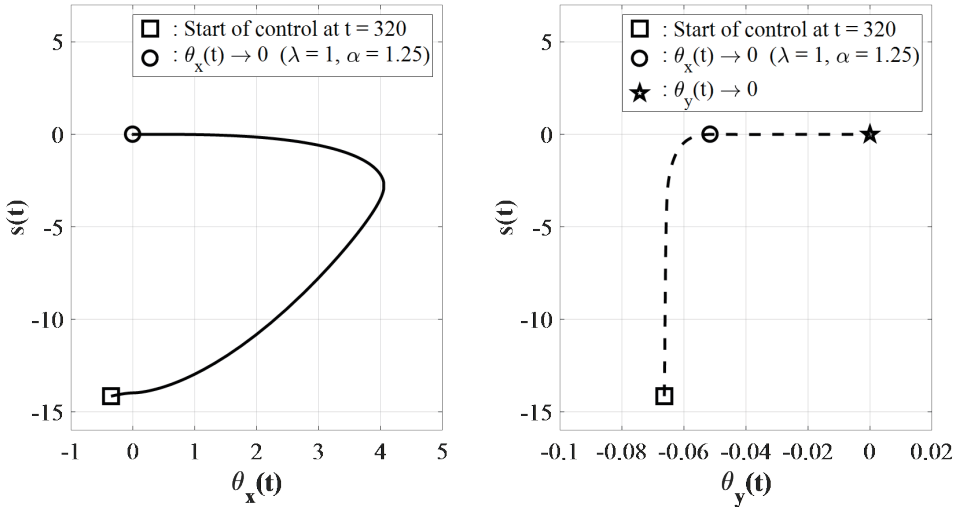

Fig. 1. Phase plane dynamics of $s(t)$ versus $\theta_x(t)$ and $\theta_y(t)$.

that $\theta_x(t)$ first converges to zero, then $\theta_y(t)$ asymptotically approaches the origin for $s(t) = 0$ associated with $\theta_x(t) = 0$. Thus, the characteristics of the IQSSM in Eq. (9) proposed in **Theorem 1** are verified. In Fig. 2, the time dynamics of $\theta_x(t)$ and $\theta_y(t)$ are shown. $\theta_x(t)$ approaches zero quickly than $\theta_y(t)$ converges. However, the control performance in this situation is not adopted in the complete synchronization due to the convergence of $\theta_y(t) \rightarrow 0$ requiring a long time.

According to Theorem 1, the performance of the control can be improved by suitably tuning the design parameters α, β. In fact, according to the results of our simulation for validation, the control performance is not sensitive to the value of β. The phase trajectories with three different values of α and the same simulation parameters for the coding as in Table 1 are demonstrated in Fig. 3. For a larger value of α, it is shown that the state $\theta_x(t)$ tends more quickly to zero when the

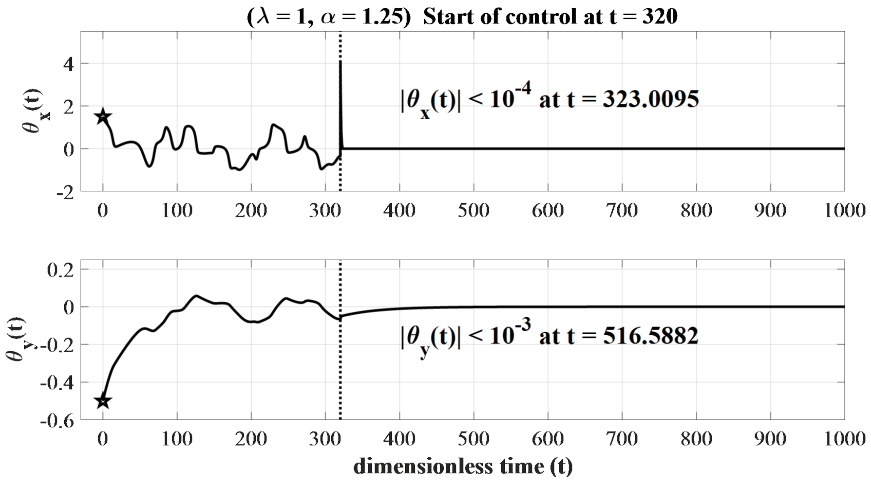

Fig. 2. Time dynamics of $\theta_x(t)$ and $\theta_y(t)$ for $\alpha = 1.25$.

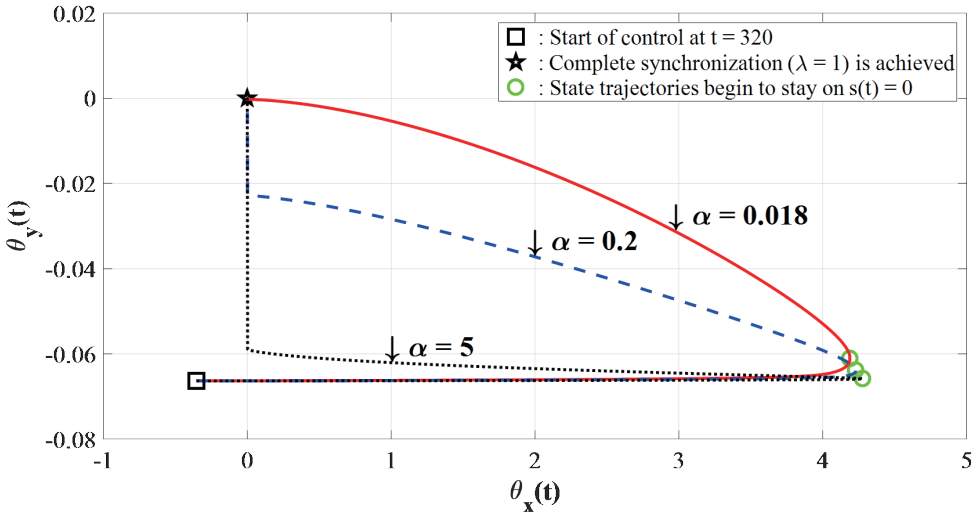

Fig. 3. (Color online) State trajectories for different values of α with $\lambda = 1$.

state trajectories begin to remain at $s(t) = 0$. Then, the state $\theta_y(t)$ subsequently converges. The nearly uniform convergence of $\theta_x(t)$ and $\theta_y(t)$ can be achieved by applying a small value of α. It is concluded that the control performance for complete synchronization can be improved by selecting a suitable value of α.

The simulation results for the case of $\lambda = 1$ with $\alpha = 0.018$, $\mu_1 = 10$, $\mu_2 = 0.15$, and $\mu_3 = 4$ are depicted in Figs. 4–6. The time dynamics of $\theta_x(t)$ and $\theta_y(t)$ are shown in Fig. 4. $\theta_x(t)$ is stabilized in a finite time after the start of control at $t = 320$. The phase trajectory arrives at $s(t) = 0$, where $\theta_x(t)$ has a peak value, at time $t = 320.2346$, where $t_0 = 0.2346$. The time required for the stabilization of $\theta_x(t)$ is estimated to be $t = t_s + t_0 = 326.995$ from the simulation. Thus, the estimated finite time required to stabilize $\theta_x(t)$ is $t_s \simeq 6.76$. From Eq. (10), the theoretical value of

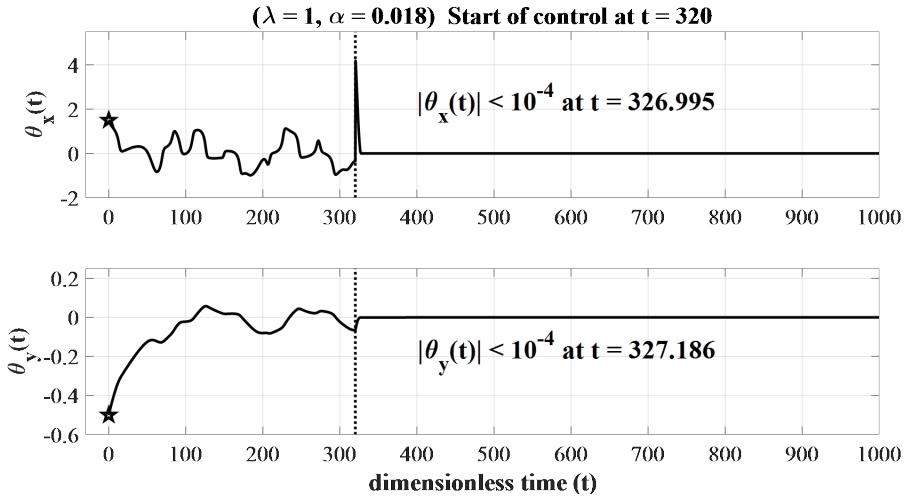

Fig. 4. Time dynamics of $\theta_x(t)$ and $\theta_y(t)$ for $\alpha = 0.018$.

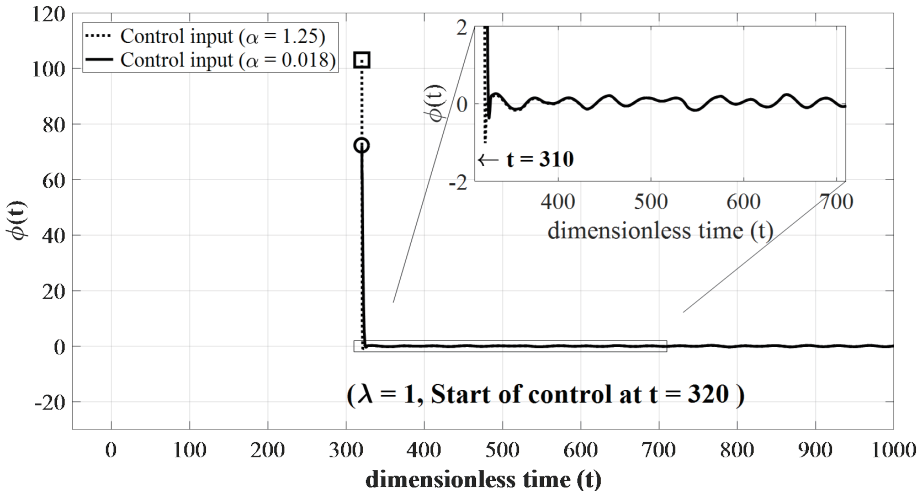

Fig. 5. Control signals of the adaptive IQSSM control for $\alpha = 0.018$, 1.25.

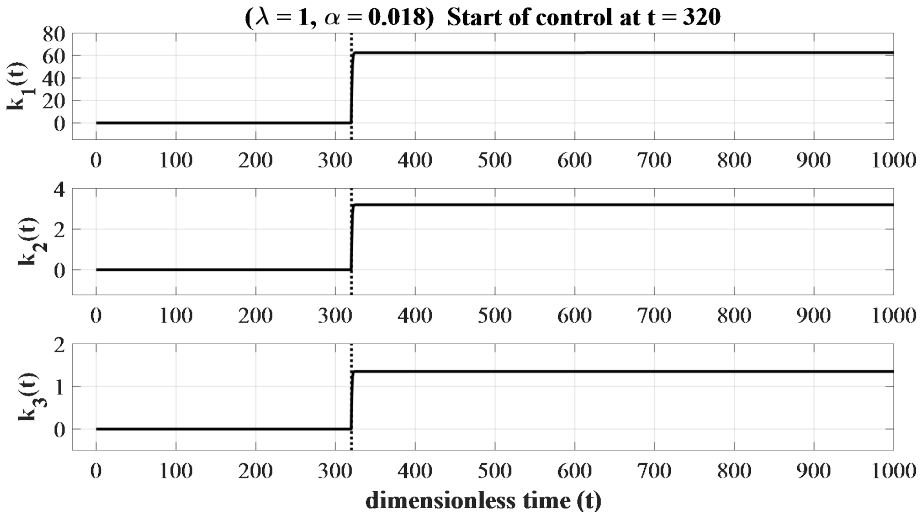

Fig. 6. Time histories of the adaptive feedback gains for $\alpha = 0.018$.

the finite time is $t_s = 6.2973$, which is basically in accordance with the estimate. After $\theta_x(t) \rightarrow 0$, $\theta_y(t)$ is then also stabilized in a short time.

Figure 5 shows that the control signals of the proposed adaptive IQSSM control for $\alpha = 0.018$, 1.25 are continuous and chatter-free. The peak value of the control for $\alpha = 0.018$ is less than that for $\alpha = 1.25$. The time histories of the three adaptive feedback gains for $\alpha = 0.018$ are shown in Fig. 6; the gains gradually approach constant values. This means that the states $\theta_x(t)$, $\theta_y(t)$, and $s(t)$ converge to zero upon applying the adaption algorithms given by Eq. (15).

For the case of $\lambda = -1$ (anti-synchronization), the simulation parameters for coding in Table 1 are also taken. The phase trajectories with three different values of α are depicted in Fig. 7. Similarly to the case of complete synchronization, it is concluded that applying small values of α can be used as a rule of thumb to achieve the nearly uniform convergence of $\theta_x(t)$ and $\theta_y(t)$. Figure 8 shows the time histories of the state variables for two isolated SFHN neurons with $\alpha = 0.012$, $\mu_1 = 1.25$, $\mu_2 = 0.005$, and $\mu_3 = 0.25$. As expected, the state variables of the two neurons in Eqs. (1) and (2) become separate from each other for the given different initial conditions. After the start of control at $t = 320$, the state variables gradually become anti-synchronized. The method proposed in Ref. 8 can only consider complete synchronization between two SFHN nerve-cell neurons. In contrast to Ref. 8, we have presented a scheme that can simultaneously solve the control problems of complete and anti-synchronization by simply tuning some design parameters.

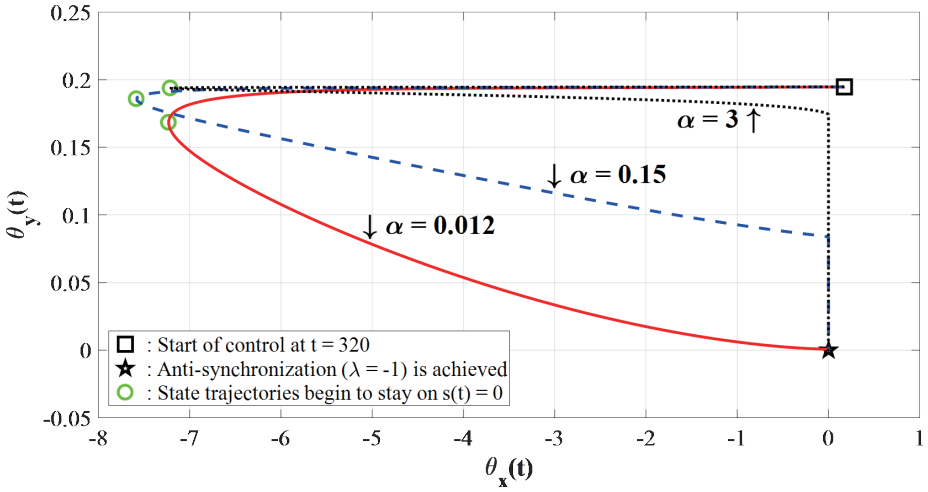

Fig. 7. (Color online) State trajectories for different values of α with $\lambda = -1$.

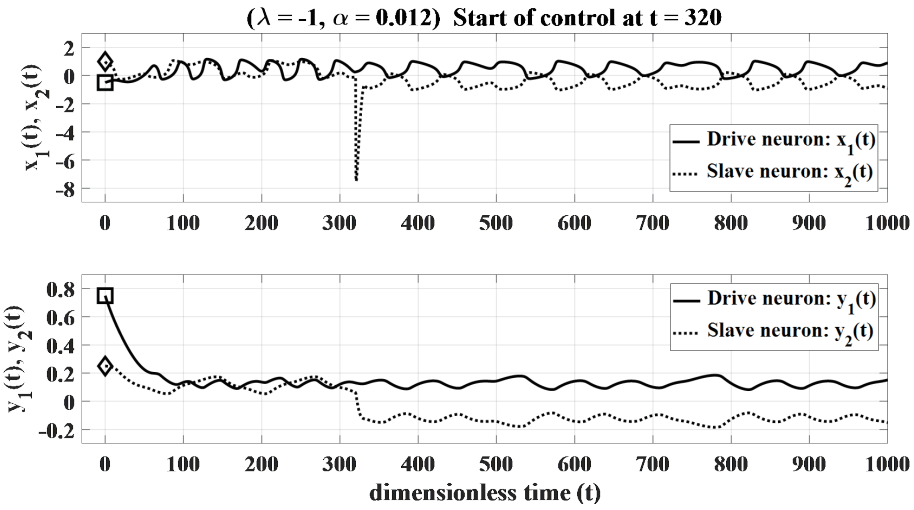

Fig. 8. Time histories of state variables for two anti-synchronous SFHN neurons.

5. Conclusions

In this study, a novel and robust adaptive IQSSM control scheme is proposed that can address complete and anti-synchronization between two isolated SFHN neurons. Theorem 1 proves that the quick finite-time stability on the sliding surface $s(t) = 0$ is guaranteed by the IQSSM. The IQSSM mainly supports the designed closed-loop control system to achieve synchronizations. The proposed adaptive control scheme involves the time-varying feedback gains, which are updated by adaptive rules, to compensate the nonlinear dynamics of the synchronous error system without directly eliminating nonlinear terms. Sufficient conditions to guarantee stable

synchronizations are given on the basis of Lyapunov stability theory. Numerical simulations are also performed to validate the proposed control scheme. It is also concluded that the control performance for the two types of synchronization can be improved by choosing suitable values of the design parameters. According to a previous study,[28] control schemes developed for synchronization can be implemented in a hardware circuit with sensing equipment. The scheme proposed in this study can be extended to other control problems in biological engineering in the future.

Acknowledgments

This work was supported by Research Funds for Introducing and Training Talents (grant number 9900064605/440) supported by Shaoguan University, the Foundation of Shaoguan Science and Technology Bureau (grant numbers 210726214533586 and 200811094530811), and National Natural Science Foundation of China (grant number 52105268). We also acknowledge support from School of Intelligent Engineering, Shaoguan University.

References

1 L. M. Pecora and T. L. Carroll: Phys. Rev. Lett. **64** (1990) 821. https://doi.org/10.1063/1.4917383
2 J. Wang, T. Zhang, and B. Deng: Chaos Solit. Fract. **31** (2007) 30. https://doi.org/10.1016/j.chaos.2005.09.006
3 X. Wei, J. Wang, and B. Deng: Commun. Nonlinear Sci. Numer. Simul. **14** (2009) 3108. https://doi.org/10.1016/j.cnsns.2008.10.016
4 M. Rehan and K. S. Hong: Phys. Lett. A **375** (2011) 1666. https://doi.org/10.1016/j.physleta.2011.03.012
5 C. C. Yang and C. L. Lin: Nonlinear Dyn. **69** (2012) 2089. https://doi.org/10.1007/s11071-012-0410-6
6 C. Han, R. Li, S. Ren, Y. Li, and Y. Che: Res. J. Appl. Sci. Eng. Tech. **5** (2013) 8509. https://doi.org/10.19026/rjaset.5.4228
7 Q. Zhang: Chaos Solit. Fract. **58** (2014) 22. https://dx.doi.org/10.1016/j.chaos.2013.11.002
8 C. Lu and X. Chen: J. Comp. Nonlinear Dyn. **11** (2016) 041011–1. https://doi.org/10.1115/1.4032074
9 H. Handa and B. B. Sharma: Nonlinear Dyn. **85** (2016) 1517. https://doi.org/10.1007/s11071-016-2776-3
10 D. Fan, X. Song, and F. Liao: Inter. J. Bifur. Chaos **28** (2018) 1850031. https://doi.org/10.1142/S0218127418500311
11 M. M. Ibrahim and H. Jung: IEEE Access **7** (2019) 57894. https://doi.org/10.1109/ACCESS.2019.2913872
12 Y. Zhang, C. N. Wang, J. Tang, J. Ma, and G. D. Ren: Sci. Chin. Tech. Sci. **63** (2020) 2328. https://doi.org/10.1007/s11431-019-1547-5
13 I. Hussain, S. Jafari, D. Ghosh, and M. Perc: Nonlinear Dyn. **104** (2021) 2711. https://doi.org/10.1007/s11071-021-06427-x
14 D. Yu, L. Lu, G. Wang, L. Yang, and Y. Jia: Chaos Solit. Fract. **147** (2021) 111000. https://doi.org/10.1016/j.chaos.2021.111000
15 A. L. Hodgkin and A. F. Huxley: J. Physiol. **117** (1952) 500. https://doi.org/10.1113/jphysiol.1952.sp004764
16 H. C. Tuckwell and J. Jost: Phys. A: Stat. Mech. Appl. **388** (2009) 4115. https://doi.org/10.1016/j.physa.2009.06.029
17 R. FitzHugh: J. Biophys. **1** (1961) 445. https://doi.org/10.1016/S0006-3495(61)86902-6
18 J. Nagumo, S. Arimoto, and S. Yoshizawa: Proc. IRE **50** (1962) 2061. https://doi.org/10.1109/JRPROC.1962.288235
19 C. J. Thompson, D. C. Bardos, Y. S. Yang, and K. H. Joyner: Chaos Solit. Fract. **10** (1999) 1825. https://doi.org/10.1016/S0960-0779(98)00131-3
20 D. Q. Wei, X. S. Luo, B. Zhang, and Y. H. Qin: Nonlinear Anal., Real World Appl. **11** (2010) 1752. https://doi.org/10.1016/j.nonrwa.2009.03.029
21 Y. Gao: Chaos Solit. Fract. **21** (2004) 943. https://doi.org/10.1016/j.chaos.2003.12.033
22 A. Petrovas, S. Lisauskas, and A. Slepikas: Elec. Electr. Eng. Kaunas: Tech. **122** (2012) 117. https://doi.org/10.5755/j01.eee.122.6.1835

23 S. Binczak, S. Jacquir, J. M. Bilbault, V. B. Kazantsev, and V. I. Nekorkin: Neural Networks **19** (2005) 684. https://doi.org/10.1016/j.neunet.2005.07.011
24 J. Cosp, S. Binczak, J. Madrenas, and D. Fernandez: Int. J. Elec. **101** (2014) 220. https://doi.org/10.1080/00207217.2013.780263
25 J. Zhao and Y. B. Kim. Proc. 2007 50th Midwest Symp. Circuits and Systems (MWSCAS, 2007) 772. https://doi.org/10.1109/MWSCAS.2007.4488691
26 Y. Hea, Q. Yang, S. Sun, M. Luo, R. Liu, and G. D. Peng: Int. J. Elec. Power Ener. Syst. **117** (2020) 105607. https://doi.org/10.1016/j.ijepes.2019.105607
27 F. C. Pereira, J. H. Galeti, R. T. Higuti, M. J. Connelly, and C. Kitano: J. Lightwave Tech. **1** (2017) 3257. https://doi.org/10.1109/JLT.2018.2840706
28 C. Y. Yeh, J. Shiu, and H. T. Yau: Math. Prob. Eng. (2012) 745396. https://doi.org/10.1155/2012/745396
29 C. C. Wang and H. T. Yau: Abs. Appl. Anal. (2013) 209718. https://doi.org/10.1155/2013/209718
30 Z. S. Zhao, J. Zhang, G. Ding, and D. K. Zhang: Acta Phys. Sin. **64** (2015) 210508. https://doi.org/10.7498/aps.64.210508
31 Z. Zhao, X. Li, J. Zhang, and Y. Pei: Inter. J. Biomath. **10** (2017) 1750041. https://doi.org/10.1142/S1793524517500413
32 Z. Zuo and L. Tie: Inter. J. Control **87** (2014) 363. https://doi.org/10.1080/00207179.2013.834484